Dependence of the Thermal Conductivity of BiFeO_{3} Thin Films on Polarization and Structure

Shuai Ning, Samuel C. Huberman, Chen Zhang, Zhengjun Zhang, Gang Chen, and Caroline A. Ross

Phys. Rev. Applied **8**, 054049 — Published 29 November 2017

DOI: 10.1103/PhysRevApplied.8.054049

Dependence of the Thermal Conductivity of $BiFeO_3$ Thin Films on Polarization and Structure

Shuai Ning[1,2], Samuel C. Huberman[3], Chen Zhang[1], Zhengjun Zhang[2], Gang Chen[3] and Caroline A. Ross[1*]

[1] Department of Materials Science and Engineering, Massachusetts Institute of Technology, Cambridge, Massachusetts 02139, USA

[2] Key Laboratory of Advanced Materials (MOE), School of Materials Science and Engineering, Tsinghua University, Beijing 100084, P. R. China

[3] Department of Mechanical Engineering, Massachusetts Institute of Technology, Cambridge, Massachusetts 02139, USA

[*] Author to whom all correspondence should be addressed. E-mail: caross@mit.edu

KEYWORDS

$BiFeO_3$, bismuth ferrite, thermal conductivity, crystalline structure, ferroelectric domain structure

ABSTRACT

The role of ferroelectric polarization state and crystal structure in determining the room temperature thermal conductivity of epitaxial $BiFeO_3$ thin films has been investigated. The ferroelectric domain configuration was varied by changing the oxygen partial pressure during growth, as well as by polarizing the samples by the application of an in-situ electric field during the thermal conductivity measurement. However, little or no dependence of thermal conductivity on the ferroelectric domain structure was observed. In contrast, the thermal conductivity did significantly depend on the morphotropic phase structure, being about 2/3 as large in tetragonal-like compared to rhombohedral-like $BiFeO_3$ film. The substantial structural dependence of thermal conductivity found here may provide a route to reversible manipulation of thermal properties.

INTRODUCTION

Manipulating the thermal properties and controlling the flow of heat in solid-state materials is of great importance for many technologies including thermal management, energy harvesting, and sensing[1]. Though there are numerous reports on the manipulation of phonon transport at room temperature through physical phase transformations[2-5], chemical composition modification[6] and defect engineering[7-9], challenges remain in reversibly tuning the thermal conductivity in a material. Recently, domain walls in ferroelectric materials, which represent coherent boundaries with a thickness of a few nanometers, have been reported in a handful of studies to have an effect on the thermal conductivity[10-12], potentially providing a method to reversibly manipulate the thermal conductivity. However, the role that ferroelectric domain walls play in tuning phonon transport is incompletely understood, and the effect of other factors including grain boundaries and other defects in

polycrystalline ferroelectric materials[10] and the substrate surface[11] complicate the analysis. Even if domain walls play a significant role, the reported magnitude of the thermal conductivity change caused by manipulating ferroelectric domains appears quite small in terms of practical applications. It is therefore of great interest to investigate the factors that affect the thermal conductivity of ferroelectric materials.

$BiFeO_3$ (BFO), a lead-free single-phase ferroelectric material, has attracted much attention owing to its interesting physical properties including multiferroicity[13]. Bulk BFO exhibits a rhombohedral structure in which oxygen octahedra are slightly tilted from the center of symmetry along the <111> pseudocubic direction. When epitaxially grown on perovskite substrates such as $SrTiO_3$ (STO), a small monoclinic distortion of the rhombohedral structure is present, and the structure is denoted as R-like BFO. In general, R-like BFO tends to polarize along the <111> directions[14], thus resulting in 8 possible domain variants with both in-plane and out of plane components, which is undesirable for practical applications. As a result, domain engineering of BFO thin films has been widely explored to improve the ferroelectric performance, such as by utilizing vicinal substrates[15,16] and tuning the buffer thickness[16,17]. Recently, a new approach for domain engineering of BFO thin films has emerged with the observation of a new polymorph with a large *c/a* ratio (~1.25) stabilized by much larger in-plane compressive strain (>4.5%)[18], which is tetragonal with a slight monoclinic distortion[19] and denoted as T-like BFO. This new polymorph is predicted to show many fascinating properties, such as a simpler switching process and higher remnant polarization. In particular, a reversible morphotropic phase transformation between R- and T-like BFO can be driven by simple stimuli[20-22], and the morphotropic phase boundary shows a strong electromechanical response[23,24].

In this paper, we investigate the thermal transport properties of epitaxial R- and T-like BFO thin films and the dependence of thermal conductivity on the polarization state. The two

polymorphs are obtained by substrate strain engineering, and the film strain state, as well as the ferroelectric domain features, are controlled via the oxygen partial pressure during deposition. The room temperature thermal conductivity is found to be almost independent of the oxygen partial pressure. Through piezoresponse force microscopy (PFM) characterization and thermal analysis with an in-situ electric field, we found the domain wall density does not play a significant role in determining the thermal conductivity, whereas the thermal conductivity is ~2/3 as great for T-like than for R-like BFO.

EXPERIMENTAL

BFO thin films of 28 - 38 nm thickness were prepared by pulsed laser deposition (PLD) using a KrF excimer laser (λ=248 nm) with 15 J/cm^2 fluence and 10 Hz pulse repetition rate, at a substrate temperature of 650 °C and under different oxygen pressures, i.e. 5 mTorr, 50 mTorr and 100 mTorr. A Bi-rich $Bi_{1.2}FeO_3$ target was used to compensate for Bi loss during deposition, and (001) oriented STO (or with 0.7 wt% Nb doping) and $LaAlO_3$ (LAO) were used as substrates. Additionally, BFO films were grown on a ~17 nm $La_{0.66}Sr_{0.33}MnO_3$ (LSMO) epitaxial layer that was firstly prepared by PLD at 800 °C under an oxygen pressure of 10 mTorr on LAO, as well as on a ~22 nm $SrRuO_3$ (SRO) layer grown at 850 °C under an oxygen pressure of 5 mTorr on LAO. The film or layer thickness was determined by X-ray reflectometry (XRR). Structural characterization was carried out by high resolution X-ray diffraction (HRXRD) and reciprocal space mapping (RSM) on a Bruker D8 Discover X-ray diffractometer. The chemical composition and defect properties were examined by X-ray photoelectron spectroscopy (XPS, ESCALAB 250Xi). The Raman spectra were measured at room temperature using a Horiba LabRAM 800 HR spectrometer equipped with a He-Ne (632.8 nm) laser as the excitation source.

The ferroelectric domain structures were characterized using PFM on a Veeco Nanoscope

V atomic force microscope operated in tapping mode and near the contact resonance of the tip-sample configuration for a better signal-to-noise ratio. A Precision Premier II Ferroelectric Tester was utilized to measure the polarization-electric (P-E) field loops at a frequency of 1 kHz with voltages of a few V. The room temperature thermal conductivity was analyzed by a homemade time domain thermoreflectance (TDTR) setup with Al layers as the transducer pads on the top of sample surface, which is sensitive to the thermal conductivity across the film plane, perpendicular to the sample surface. The in-situ TDTR measurements were conducted with a layer of Au (100 nm)/Ta (5 nm) as the transducer pads, which were prepared by sputtering with a diameter of 150 μm. The Precision Premier II Ferroelectric Tester was used to apply the DC bias for the in situ TDTR measurements, via a probe station contacting the Au/Ta pads.

RESULTS AND DISSCUSSION

Structural characterizations by HRXRD are summarized in Fig. 1. No secondary phase peaks can be seen, indicating that single phase BFO is obtained in each case. Comparing the XRD results of BFO films grown at 5 mTorr on different substrates, one may see that the crystalline structure can be effectively manipulated by substrate strain engineering. Specifically, the ~30 nm BFO film grown on STO, as well as on SRO/LAO, exhibits a typical R-like structure, while that grown on LAO and LSMO/LAO has a qualitatively different diffraction pattern corresponding to T-like BFO. A slight shift of the BFO diffraction peak shown in both Fig. 1(a) and (b) suggests the BFO films grown on bare substrates and on a bottom layer were under different strain states.

Reciprocal space mapping was collected in the same instrument using the asymmetric (103) or (113) family of peaks. The split of the (103) signals of the T-like BFO shown in Fig. S1 of Ref. [25] clearly indicates a slight monoclinic distortion along the <100> direction[23].

The structural information interpreted from RSM analysis (see Table 1) demonstrates a significant structural difference between the two polymorphs seen in the much larger *c/a* ratio and unit cell volume in T-like BFO compared to R-like BFO, as illustrated by the ideal crystalline structure shown in the inset of Fig. 1(a) and (b). Meanwhile, the R-like BFO grown on SRO/LAO shows more relaxation in comparison with that on STO, due to the larger in-plane lattice parameters of the SRO layer on LAO compared to the STO bare substrate. For T-like BFO, there is little difference between film peak positions for samples on LSMO/LAO and on LAO, as a consequence of the similar in-plane lattice parameters of the LSMO layer and the LAO bare substrate.

Additionally, T-like BFO films were grown on LAO and R-like films were grown on STO under oxygen pressures of 5, 50 and 100 mTorr. Adjusting the oxygen partial pressure during deposition did not change the crystalline structure, but impact the strain state suggested by the clear shift of the diffraction peaks shown in Fig. 1(c) and (d). The detailed structural information shown in Table 1, as well as Fig. S1 of Ref. [25], clearly shows that higher oxygen pressure leads to a smaller out of plane lattice parameter and a larger in-plane lattice parameter, but little change in the unit cell volume, and more relaxation occurs when grown under higher oxygen pressure.

The room temperature thermal conductivity was analyzed by TDTR methods as described elsewhere [26-28], and further details are given in Ref. [25]. The thermal conductivities of the underlying layers (LSMO and SRO) and the bare substrates (STO and LAO) were first analyzed, and then used as known with other input parameters [29-33] in the non-linear least squares minimization fitting procedure to obtain the cross-plane thermal conductivity of BFO thin films. Fig. 2 shows the room temperature thermal conductivity of 4 pairs of BFO samples. Each pair is from the same deposition run and has the same film thickness. Comparing the results of BFO/STO and BFO/SRO/LAO grown under the same oxygen

pressure, as well as BFO/LAO and BFO/LSMO/LAO, one can observe that the thermal conductivity is independent of the underlayers or substrates, indicating that the fitting procedure of the TDTR data analysis is reasonable. Besides that, two interesting phenomena can be seen. First, the thermal conductivity is almost independent of the oxygen pressure for each polymorph despite the varying film strain states. Second, the thermal conductivity is significantly dependent on the crystal structure, with the value of T-like BFO consistently ~2/3 that of R-like BFO.

Chemical composition and defect properties were examined by high resolution XPS on three representative samples, i.e. T-like BFO/LAO grown at 5 mTorr, and R-like BFO/STO grown at 5 mTorr and 100 mTorr, denoted as T-5, R-5 and R-100 respectively. Before measurements, all samples were sputtered by Ar^+ for 5 minutes to remove surface contamination. From the XPS of Bi shown in Fig. 3(a), one can see all samples exhibit two pairs of 4f peaks: the one with higher binding energy corresponds to Bi^{3+}, and the other one with lower binding energy corresponds to Bi with a lower valence state, probably created by the Ar^+ sputtering. The Fe 2p core level spectra can be fitted by one pair of peaks shown in Fig. 3(c). Together with the satellite features of Fe 2p, one can expect the Fe elements are in a +3 valence state. Additionally, the well-fitted symmetric peaks of the O 1s core level shown in Fig. 3(b) indicate the amount of oxygen vacancies is quite low. One should note that the peak position and relative intensity of Bi, O and Fe seem very similar in R-5 and R-100, which means the defect states of samples do not differ greatly with the oxygen partial pressure during PLD.

The ferroelectric domain features were examined by PFM, which is sensitive to the out-of-plane component of the polarization, on four representative samples, i.e. T-like BFO/LSMO/LAO grown at 5 mTorr and 100 mTorr, and R-like BFO/Nb:STO grown at 5 mTorr and 100 mTorr, denoted as T-5, T-100, R-5 and R-100 respectively. The R-like

BFO/Nb:STO was used for PFM characterization instead of R-like BFO/SRO/LAO because the surface of the latter has higher roughness. There is no difference in the BFO peak position between films on STO and on Nb:STO (see Fig. S3 in Ref. [25]).

Fig. 4 shows the PFM phase images, where contrast can be clearly seen in all the samples, indicating ferroelectric domains with different out-of-plane component coexist in each as-grown sample. A stripe-like domain structure can be seen in both T-like samples, while a qualitatively different mosaic-like domain pattern exists in R-like samples. The domain size, shape and density vary considerably with oxygen pressure during deposition, suggesting that adjusting oxygen pressure during deposition can be an approach to domain engineering in both R- and T-like polymorphs[34]. This may be a result of changes in the surface chemistry during growth at different oxygen pressures in order to achieve charge compensation and maintain the polarization[35, 36], or a consequence of structural relaxation. The micrometers-long stripes in T-100 shown in Fig. 4(b) appear to be much narrower than those in T-5 (see Fig. 4(a)), thus leading to a much higher domain wall density. Meanwhile, both of them exhibit a weak vertical PFM contrast, indicating those domains might have an in-plane polarization component due to a deviation of the ferroelectric axis from the c-axis[37]. As for R-like samples, the domains of R-5 are more random, much smaller, and of a higher density than R-100. As suggested by previous work[38], the phase image of R-5 in Fig. 4(c) indicates 8 possible domain variants might coexist, resulting in 3 possible polarization angles at the domain walls (180°, 71° and 109° boundaries, where the latter two are ferroelastic) which can be charged or neutral. In comparison, the image of R-100 in Fig. 4(d) is characteristic of a system with fewer possible domain variants[11] and lower domain wall density. The slightly lower thermal conductivity of R-5 (1.29 $Wm^{-1}K^{-1}$) compared to R-100 (1.32 $Wm^{-1}K^{-1}$), as well as the lower thermal conductivity of T-100 (0.82 $Wm^{-1}K^{-1}$) compared to T-5 (0.84 $Wm^{-1}K^{-1}$), could be a consequence of the contribution of domain walls to phonon scattering,

although this effect seems to be negligibly small.

The ferroelectric hysteresis of both R-5 and T-5 was measured using the PFM. Typical out-of-plane P-E loops were obtained in both cases shown in Fig. 5(a) and (b). The larger coercivity and weaker piezoresponse suggests a more complicated polarization switching mechanism in R-like BFO samples. A DC bias of +6 V/-6 V, which seemed sufficient to polarize both BFO polymorph films based on the hysteresis loops, was used to conduct the writing and re-writing switching experiments. The respective phase images were immediately collected after removing the bias. The clear phase contrast shown in Fig. 5(c) and (d) indicates both R- and T-like BFO samples can be polarized and switched at a bias of ~6 V, and that the domain wall density can be significantly tuned by the external electric field.

To further investigate the role that domain walls play in determining the thermal conductivity, in-situ TDTR measurements, in which the thermal analysis is performed simultaneously with changing the domain configuration, are valuable. The layout of the PFM instrument precludes access by the TDTR laser, so instead the in situ measurements were done by applying the DC bias through top electrodes during the TDTR measurement as shown schematically in Fig. 5(e). Out-of-plane P-E loops were first measured within the in-situ TDTR setup (see Fig. S4 in Ref. [25]) showing that both R- and T-like samples can be polarized by a DC bias, i.e. the domain wall density will change significantly during application of a voltage. Basically, the domain wall can be in three different configurations. Walls such as Fig 6(c), orthogonal to the heat flow, are expected to affect heat flow analogous to the interfaces of a multilayered film affecting cross-plane thermal conductivity. However, given the small film thickness, we expect most domain walls to be oriented through the film thickness which is parallel or at an angle to the direction of heat flow in the TDTR measurements as in Fig. 6(a) and (b) respectively.

In-situ TDTR data were collected on both T-5 and R-5 samples (see Fig. S5 in Ref. [25]).

The results shown in Fig. 5(f) suggest the conductivity of the R-like BFO film is slightly reduced or unchanged with an applied bias, while that of the T-like BFO does not show a clear decrease considering the limits in accuracy of the measurement. For T-like (001) epitaxial BFO films which are predicted to be polarized out-of-plane, it is possible that the insensitivity of thermal conductivity to domain wall density in the in-situ experiment occurs because polarization changes are accomplished by movement of only 180° walls which are not ferroelastic and would not be expected to interact strongly with phonons due to no structural distortion. As for R-like (001) BFO epitaxial films, however, prior work has shown that an out-of-plane voltage can result in not only 180° switching, but also 71° and 109°. The phase-field simulation suggests that the activation energy for direct 180° switching is higher than that for 71°, leading to a relaxation-mediated 180° switching path for R-like BFO in which the out-of-plane electric field induced 71° switching, and the unstable 71° domains then relax into the stable 180˚ ones at remanence [39]. Further experimental study indicated a phase-dependent switching mechanism in R-like BFO in which ferroelastic polarization rotations (71˚ or 109˚) become dominant as the applied bias increases, instead of ferroelectric switching (180˚), whereas switching using a top electrode only leads to ferroelastic switching. This is because electrodes with larger area could stabilize 71˚ domains due to larger domain size [39-41]. The 150 μm top electrodes we utilized in the in-situ TDTR measurement can plausibly involve substantial ferroelastic domain walls, which could contribute to the phonon scattering and the reduce of thermal conductivity. However, the observed decrease of thermal conductivity is quite small, indicating that the domain wall density has a relatively minor influence on the thermal conductivity.

As to the significant dependence of thermal conductivity on the polymorph, it may originate from the differences in structure and ionic coordination. Raman measurements were carried out at room temperature. From the results shown in Fig. 7(a) and (b), five Raman

peaks from the BFO/STO sample can be identified as typical phonon modes of R-like BFO with *R3c* symmetry, while 7 peaks from the BFO/LAO sample can be clearly ascribed to T-like BFO with *Cc* symmetry [42, 43]. The peaks in the R-like BFO film are superposed on a strong fluorescence signal from the STO substrate but weak peaks are evident as seen in the thin BFO films of Ref. [44]. The larger number of phonon modes in T-like BFO suggested by previous theoretical calculations [42] can make more contribution to thermal scattering. Therefore, the thermal conductivity of T-like BFO should be lower than that of R-like BFO. Besides, the distortion of oxygen octahedra caused by the larger *c/a* ratio may lead to a much weaker Fe-O bonding along the <001> direction in T-like BFO. The reduced thermal conductivity of T-like BFO can be also understood as a result of this weaker inter-layer coupling and increased anharmonicity for T-like BFO.

CONCLUSION

Two different polymorphs of PLD-grown epitaxial BFO thin films, i.e. R-like and T-like BFO, were obtained by substrate strain engineering. The as-grown ferroelectric domain features of each polymorph are quite different: T-like BFO shows a periodic stripe-like domain pattern, while R-like shows a mosaic domain structure. The oxygen pressure has a substantial effect on the ferroelectric domain morphology for each polymorph, providing a convenient method for domain engineering. However, the oxygen partial pressure during deposition had only modest influence on the film strain and defect levels, which are predicted to influence the thermal conductivity[45, 46].

There was little difference in thermal conductivity with oxygen pressure suggesting that the domain configuration for either R-like or T-like samples did not greatly influence the thermal conductivity. Further in-situ TDTR analysis, in which the domain state was changed by applying a voltage during the thermal conductivity measurement, also supports the

conclusion that domain wall density in the films and geometry studied here has only minor effects on the thermal transport. However, a substantial dependence of thermal conductivity on the morphotropic phase structure was observed. The thermal conductivity of T-like BFO is about 2/3 that of R-like BFO. In comparison with the effects of domain walls in our work, as well as that reported in Ref [11], the structural dependence of thermal conductivity observed here is a much greater effect, suggesting that the morphotropic phase transformation could be used to control the thermal properties of BFO thin films.

ACKNOWLEDGMENT

This work was sponsored by the Solid-State Solar-Thermal Energy Conversion Center (S3TEC) under award DE-SC0001299. Shared facilities of the MIT MRSEC through the MRSEC Program of the National Science Foundation under Award No. DMR-1419807 were used.

REFERENCE

[1] E. S. Toberer, L. L. Baranowski, and C. Dames, Advances in thermal conductivity, Annu. Rev. Mater. Res. **42**, 179 (2012).

[2] D.-W. Oh, C. Ko, S. Ramanathan, and D. G. Cahill, Thermal conductivity and dynamic heat capacity across the metal-insulator transition in thin film VO 2, Appl. Phys. Lett. **96**, 151906 (2010).

[3] R. Zheng, J. Gao, J. Wang, and G. Chen, Reversible temperature regulation of electrical and thermal conductivity using liquid–solid phase transitions, Nat. Commun. **2**, 289 (2011).

[4] H. Ji, D. P. Sellan, M. T. Pettes, X. Kong, J. Ji, L. Shi, and R. S. Ruoff, Enhanced thermal conductivity of phase change materials with ultrathin-graphite foams for thermal energy storage, Energy Environ. Sci. **7**, 1185 (2014).

[5] Z. Guo, S. J. Yoon, J. S. Manser, P. V. Kamat, and T. Luo, Structural phase-and degradation-dependent thermal conductivity of CH3NH3PbI3 perovskite thin films, The J. Phys. Chem. C **120**, 6394 (2016).

[6] J. Cho, M. D. Losego, H. G. Zhang, H. Kim, J. Zuo, I. Petrov, D. G. Cahill, and P. V. Braun, Electrochemically tunable thermal conductivity of lithium cobalt oxide, Nat. Commun. **5** (2014).

[7] S. Dhara, H. S. Solanki, V. Singh, S. Sengupta, B. Chalke, A. Dhar, M. Gokhale, A. Bhattacharya, and M. M. Deshmukh, Tunable thermal conductivity in defect engineered nanowires at low temperatures, Phys. Rev. B **84**, 121307 (2011).

[8] K. E. Meyer, R. Cheaito, E. Paisley, C. T. Shelton, J. L. Braun, J.-P. Maria, J. F. Ihlefeld, and P. E. Hopkins, Crystalline coherence length effects on the thermal conductivity of MgO thin films, J. Mater. Sci. **51**, 10408 (2016).

[9] B. F. Donovan, E. Sachet, J.-P. Maria, and P. E. Hopkins, Interplay between mass-impurity and vacancy phonon scattering effects on the thermal conductivity of doped cadmium oxide, Appl. Phys. Lett. **108**, 021901 (2016).

[10] J. F. Ihlefeld, B. M. Foley, D. A. Scrymgeour, J. R. Michael, B. B. McKenzie, D. L. Medlin, M. Wallace, S. Trolier-McKinstry, and P. E. Hopkins, Room-temperature voltage tunable phonon thermal conductivity via reconfigurable interfaces in ferroelectric thin films, Nano Lett. **15**, 1791 (2015).

[11] P. E. Hopkins, C. Adamo, L. Ye, B. D. Huey, S. R. Lee, D. G. Schlom, and J. F. Ihlefeld, Effects of coherent ferroelastic domain walls on the thermal conductivity and Kapitza conductance in bismuth ferrite, Appl. Phys. Lett. **102**, 121903 (2013).

[12] J.-J. Wang, Y. Wang, J. F. Ihlefeld, P. E. Hopkins, and L.-Q. Chen, Tunable thermal conductivity via domain structure engineering in ferroelectric thin films: A phase-field simulation, Acta Mater. **111**, 220 (2016).

[13] T. Zhao, A. Scholl, F. Zavaliche, K. Lee, M. Barry, A. Doran, M. Cruz, Y. Chu, C. Ederer, and N. Spaldin, Electrical control of antiferromagnetic domains in multiferroic BiFeO3 films at room temperature, Nat. Mater. **5**, 823 (2006).

[14] G. Catalan and J. F. Scott, Physics and applications of bismuth ferrite, Adv. Mater. **21**, 2463 (2009).

[15] Y. H. Chu, M. P. Cruz, C. H. Yang, L. W. Martin, P. L. Yang, J. X. Zhang, K. Lee, P. Yu, L. Q. Chen, and R. Ramesh, Domain control in multiferroic BiFeO3 through substrate vicinality, Adv. Mater. **19**, 2662 (2007).

[16] Y.-H. Chu, Q. He, C.-H. Yang, P. Yu, L. W. Martin, P. Shafer, and R. Ramesh, Nanoscale control of domain architectures in BiFeO3 thin films, Nano Lett. **9**, 1726 (2009).

[17] M. Trassin, G. D. Luca, S. Manz, and M. Fiebig, Probing ferroelectric domain engineering in BiFeO3 thin films by second harmonic generation, Adv. Mater. **27**, 4871 (2015).

[18] R. Zeches, M. Rossell, J. Zhang, A. Hatt, Q. He, C.-H. Yang, A. Kumar, C. Wang, A. Melville, and C. Adamo, A strain-driven morphotropic phase boundary in BiFeO3, Science **326**, 977 (2009).

[19] H. M. Christen, J. H. Nam, H. S. Kim, A. J. Hatt, and N. A. Spaldin, Stress-induced R− M A− M C− T symmetry changes in BiFeO 3 films, Phys. Rev. B **83**, 144107 (2011).

[20] D. Mazumdar, V. Shelke, M. Iliev, S. Jesse, A. Kumar, S. V. Kalinin, A. P. Baddorf, and A. Gupta, Nanoscale switching characteristics of nearly tetragonal BiFeO3 thin films, Nano Lett. **10**, 2555 (2010).

[21] C. Beekman, W. Siemons, T. Z. Ward, M. Chi, J. Howe, M. D. Biegalski, N. Balke, P. Maksymovych, A. Farrar, and J. Romero, Phase transitions, phase coexistence, and piezoelectric switching behavior in highly strained BiFeO3 films, Adv. Mater. **25**, 5561 (2013).

[22] C.-H. Chiu, W.-I. Liang, C.-W. Huang, J.-Y. Chen, Y.-Y. Liu, J.-Y. Li, C.-L. Hsin, Y.-H. Chu, and W.-W. Wu, Atomic Visualization of the Phase Transition in Highly Strained BiFeO 3 Thin Films with Excellent Pyroelectric Response, Nano Energy **17**, 72 (2015).

[23] A. J. Hatt, N. A. Spaldin, and C. Ederer, Strain-induced isosymmetric phase transition in BiFeO 3, Phys. Rev. B **81**, 054109 (2010).

[24] J. Zhang, Q. He, M. Trassin, W. Luo, D. Yi, M. Rossell, P. Yu, L. You, C. Wang, and C. Kuo, Microscopic origin of the giant ferroelectric polarization in tetragonal-like BiFeO 3, Phys. Rev. Lett. **107**, 147602 (2011).

[25] See the Supplemental Material at [URL will be inserted by publisher] for RSM analysis, TDTR methods, P-E loops and raw data for in-situ TDTR measurements.

[26] W. S. Capinski and H. J. Maris, Improved apparatus for picosecond pump - and - probe optical measurements, Rev. Sci. Instrum. **67**, 2720 (1996).

[27] D. G. Cahill, K. Goodson, and A. Majumdar, Thermometry and thermal transport in micro/nanoscale solid-state devices and structures, J. Heat Transfer **124**, 223 (2002).

[28] A. J. Schmidt, X. Chen, and G. Chen, Pulse accumulation, radial heat conduction, and anisotropic thermal conductivity in pump-probe transient thermoreflectance, Rev. Sci. Instrum. **79**, 114902 (2008).

[29] J. Chen, W. Wang, J.-B. Li, and G. Rao, X-ray diffraction analysis and specific heat capacity of (Bi 1− x La x) FeO 3 perovskites, J. Alloys Compd. **459**, 66 (2008).

[30] L.-M. Wang, J.-H. Lai, J.-I. Wu, Y.-K. Kuo, and C. Chang, Effects of Ru substitution for Mn on La 0.7 Sr 0.3 MnO 3 perovskites, J. Appl. Phys. **102**, 023915 (2007).

[31] F. Castelpoggi, L. Morelli, H. Salva, S. Cuffini, R. Carbonio, and R. Sanchez, Specific heat measurement of the magnetoresistant perovskite SrRuO3, Solid State Commun. **101**, 597 (1997).

[32] A. Durán, F. Morales, L. Fuentes, and J. Siqueiros, Specific heat anomalies at 37, 105 and 455 K in SrTiO3: Pr, J. Phys.: Condens. Matter **20**, 085219 (2008).

[33] W. Schnelle, R. Fischer, and E. Gmelin, Specific heat capacity and thermal conductivity of NdGaO3 and LaAlO3 single crystals at low temperatures, J. Phys. D: Appl. Phys. **34**, 846 (2001).

[34] M. Highland, T. Fister, D. Fong, P. Fuoss, C. Thompson, J. Eastman, S. Streiffer, and G. Stephenson, Equilibrium polarization of ultrathin PbTiO3 with surface compensation controlled by oxygen partial pressure, Phys. Rev. Lett. **107**, 187602 (2011).

[35] R. V. Wang, D. D. Fong, F. Jiang, M. J. Highland, P. H. Fuoss, C. Thompson, A. M. Kolpak, J. A. Eastman, S. K. Streiffer, A. M. Rappe, and G. B. Stephenson, Reversible chemical switching of a ferroelectric film, Phys. Rev. Lett. **102**, 047601 (2009).

[36] M. J. Highland, T. T. Fister, M. I. Richard, D. D. Fong, P. H. Fuoss, C. Thompson, J. A. Eastman, S. K. Streiffer, and G. B. Stephenson, Polarization switching without domain formation at the intrinsic coercive field in ultrathin ferroelectric PbTiO3, Phys. Rev. Lett. **105**, 167601 (2010).

[37] H.-J. Liu, Y.-H. Du, P. Gao, Y.-C. Huang, H.-W. Chen, Y.-C. Chen, H.-L. Liu, Q. He, Y. Ikuhara, and Y.-H. Chu, Tetragonal BiFeO3 on yttria-stabilized zirconia, APL Mater. **3**, 116104 (2015).

[38] J. Desmarais, J. F. Ihlefeld, T. Heeg, J. Schubert, D. G. Schlom, and B. D. Huey, Mapping and statistics of ferroelectric domain boundary angles and types, Appl. Phys. Lett. **99**, 162902 (2011).

[39] S. Baek, H. Jang, C. Folkman, Y. Li, B. Winchester, J. Zhang, Q. He, Y. Chu, C. Nelson, and M. Rzchowski, Ferroelastic switching for nanoscale non-volatile magnetoelectric devices, Nat. Mater. **9**, 309 (2010).

[40] F. Zavaliche, P. Shafer, R. Ramesh, M. Cruz, R. Das, D. Kim, and C. Eom, Polarization switching in epitaxial Bi Fe O 3 films, Appl. Phys. Lett. **87**, 252902 (2005).

[41] M. Cruz, Y. Chu, J. Zhang, P. Yang, F. Zavaliche, Q. He, P. Shafer, L. Chen, and R. Ramesh, Strain control of domain-wall stability in epitaxial BiFeO 3 (110) films, Phys. Rev. Lett. **99**, 217601 (2007).

[42] M. Iliev, M. Abrashev, D. Mazumdar, V. Shelke, and A. Gupta, Polarized Raman spectroscopy of nearly tetragonal BiFeO 3 thin films, Phys. Rev. B **82**, 014107 (2010).

[43] G. Khabiri, A. Anokhin, A. Razumnaya, Y. I. Yuzyuk, I. Gueye, B. Carcan, H. Bouyanfif, J. Wolfman, C. Autret-Lambert, and M. El Marssi, Phonon and magnon excitations in Raman spectra of an epitaxial bismuth ferrite film, Phys. Solid State **56**, 2507 (2014).

[44] H. Béa, M. Bibes, S. Petit, J. Kreisel, and A. Barthélémy, Structural distortion and magnetism of BiFeO3 epitaxial thin films: a Raman spectroscopy and neutron diffraction study, Philos. Mag. Lett. **87**, 165 (2007).

[45] X. Li, K. Maute, M. L. Dunn, and R. Yang, Strain effects on the thermal conductivity of nanostructures, Phys. Rev. B **81**, 245318 (2010).

[46] S. Kumar, D. Garcia, J. Jin, and A. Haque, Mechanical strain mediated carrier scattering and its role in charge and thermal transport in freestanding nanocrystalline aluminum thin films, J. Vac. Sci. Technol. B **33**, 022002 (2015).

Table 1. The structural characterization results of BFO films on different substrates

Sample	BFO phase	Substrate lattice parameter (Å)	BFO film lattice parameter (Å)	Unit cell volume ($Å^3$)	*c/a* ratio
BFO/STO-5 mTorr	R-like	a_{STO}=c_{STO}= 3.905	*a*=3.900 *c*=4.093	62.25	1.049
BFO/STO-100 mTorr	R-like	a_{STO}=c_{STO}= 3.905	*a*=3.904 *c*=4.067	61.98	1.042
BFO/SRO/LAO-5mTorr	R-like	a_{SRO}=3.947 c_{SRO}=3.930	*a*=3.942 *c*=3.930	61.07	0.997
BFO/STO-5 mTorr	T-like	a_{LAO}=c_{LAO}= 3.788	*a*=3.778 *c*=4.689	66.93	1.241
BFO/STO-100 mTorr	T-like	a_{LAO}=c_{LAO}= 3.788	*a*=3.783 *c*=4.621	66.13	1.222
BFO/SRO/LAO-5 mTorr	T-like	a_{LSMO}=3.776 c_{LSMO}=4.007	*a*=3.772 *c*=4.710	67.10	1.249

Fig. 1.

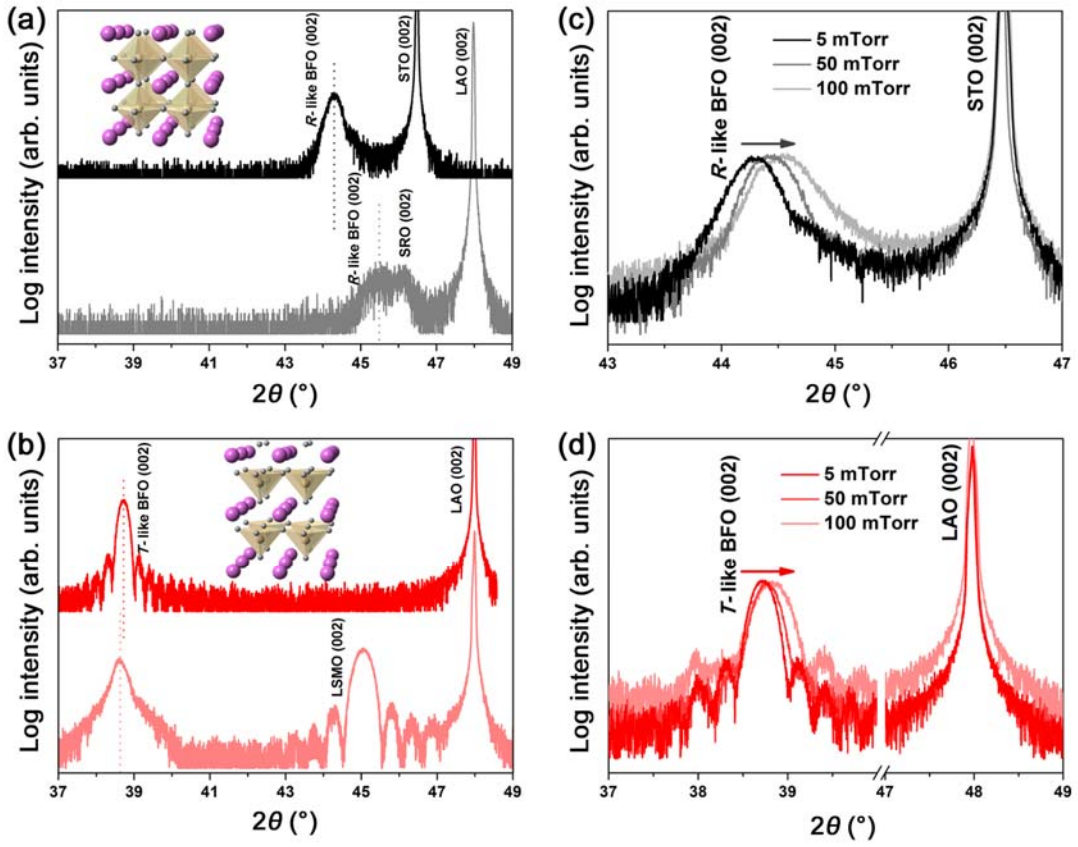

Fig. 1. HRXRD structural characterizations: (a) R-like BFO films grown on STO and SRO/LAO at 5 mTorr oxygen; (b) T-like BFO films grown on LAO and LSMO/LAO at 5 mTorr oxygen; (c) R-like BFO films on STO and (d) T-like BFO films on LAO grown under different oxygen partial pressures of 5, 50 and 100 mTorr. The ideal crystalline structure of rhombohedral BFO and tetragonal BFO is shown in the insets of (a) and (b), respectively.

Fig. 2.

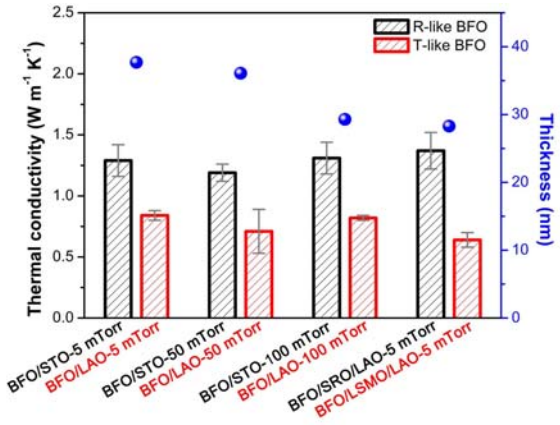

Fig. 2. Room temperature thermal conductivity analyzed by TDTR and BFO thickness by XRR of both R- and T-like BFO films prepared on different substrates and under different oxygen partial pressures.

Fig. 3.

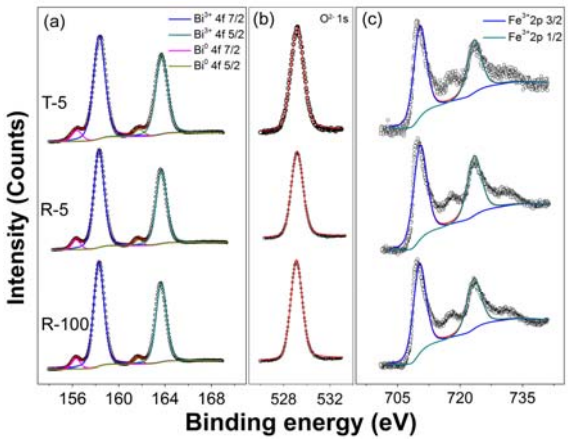

Fig. 3. High resolution XPS analysis of (a) Bi, (b) O and (c) Fe in samples T-5, R-5 and R-100.

Fig. 4.

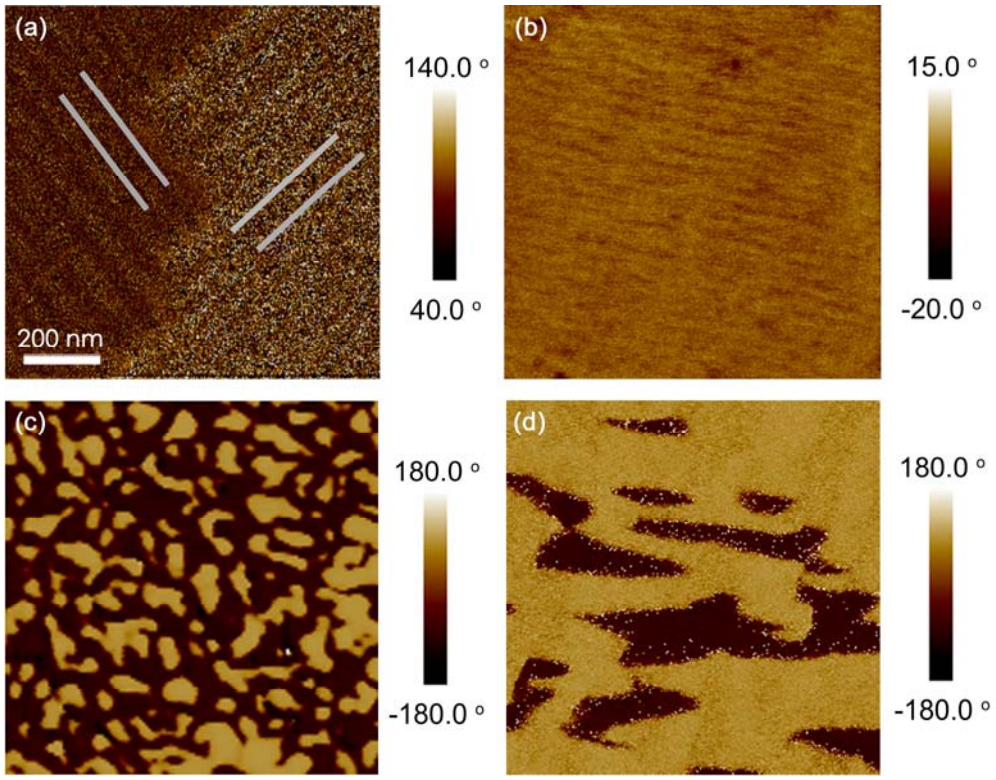

Fig. 4. Vertical PFM phase images of (a) T-5, (b) T-100, (c) R-5, and (d) R-100.

Fig. 5.

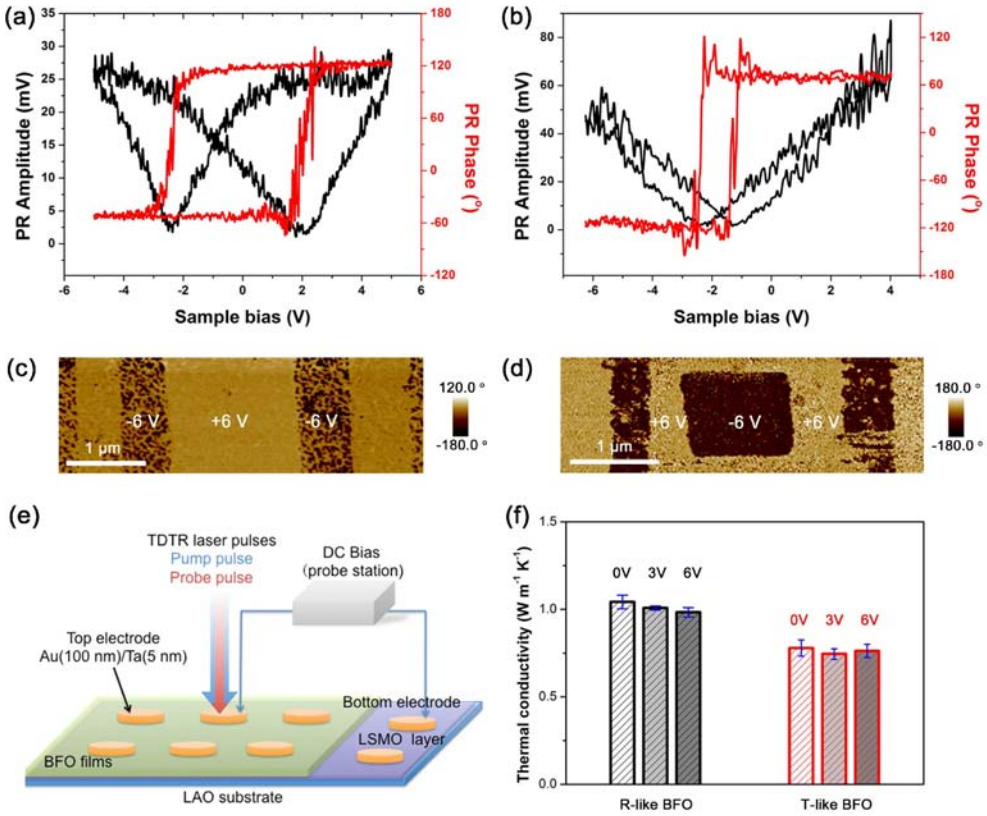

Fig. 5. In-situ TDTR analysis: Local PE amplitude and phase data measured by PFM of (a) R-like BFO(30 nm)/Nb:STO and (b) T-like BFO(30 nm)/LSMO(17 nm)/LAO grown under an oxygen pressure of 5 mTorr; The writing and re-writing switching PFM phase images of (c) R-like and (d) T-like BFO; (e) The schematic of in-situ TDTR measurements; (f) The thermal conductivity of both R- and T-like BFO samples from in-situ TDTR measurements.

Fig. 6

Fig. 6. Possible domain wall configurations: (a) normal, (b) oblique, and (c) parallel to the surface of sample.

Fig. 7.

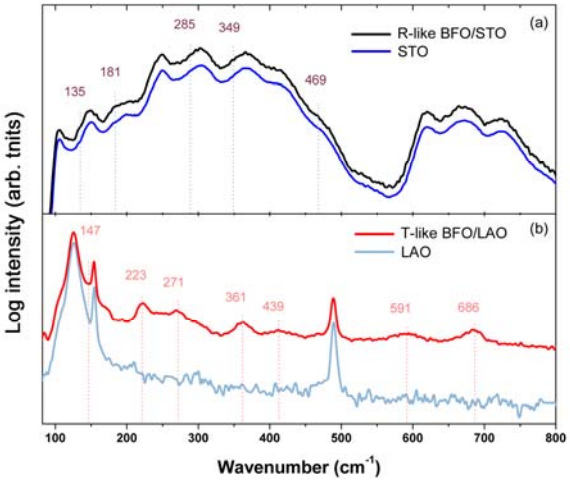

Fig. 7. Raman spectra of (a) R-like and (b) T-like BFO thin films and bare substrates.